

## ABUNDANCES IN H II REGIONS AT THE EDGE OF THE GALAXY

MICHEL FICH

Guelph-Waterloo Program for Graduate Work in Physics, University of Waterloo

AND

MARIABETH SILKEY

Hatfield and Dawson Consulting Electrical Engineers

Received 1990 April 9; accepted 1990 June 27

### ABSTRACT

Optical spectra, supplemented by some observations of radio recombination lines, have been used to estimate the abundances of helium, oxygen, nitrogen, sulfur, and argon in 18 H II regions in the outer Galaxy. Assuming that  $R_0$  (the distance from the center of the Galaxy to the Sun) is 8.5 kpc, these H II regions are located between 11.5 and 17.9 kpc from the Galactic center and include many of the most distant (from the center) H II regions known in our Galaxy. The single most striking result of these observations is the apparent high nitrogen abundances in the H II regions at the outer edge of the visible disk of the Galaxy.

*Subject headings:* abundances — galaxies: The Galaxy — nebulae: H II regions

### I. INTRODUCTION

The relative abundances of the chemical elements and their isotopes in the interstellar medium vary with position within galaxies and between one galaxy and another. These abundances vary with time as well. Stars continually enrich the interstellar medium with the products of the nucleosynthesis occurring at their cores. Knowledge of the relative abundances of the elements is critical to our understanding of the physics of the interstellar medium. Measurements of these abundances can then provide us with vital clues to the understanding of star formation rates, initial mass functions, stellar evolution, and the process of nucleosynthesis itself. Moreover, measurements of the gradient in these abundances will improve our understanding of the evolution of the Galaxy as a whole.

Galactic abundance gradients in the interstellar medium were first described by Searle (1971) in a survey of H II regions in six Sc galaxies. Early work in our Galaxy includes that of Peimbert, Torres-Peimbert, and Rayo (1978) and Hawley (1978), who found nitrogen gradients  $d \log N(H)/dR = -0.23$  and  $-0.10 \text{ kpc}^{-1}$ , respectively.

In the definitive paper on the subject by Shaver *et al.* (1983, hereafter SMNDP) observations of H II regions were used to measure the abundance gradient of our Galaxy in several elements. They thoroughly discuss the many issues involved in the determination of the abundance gradient and carefully describe a method for making this determination. Their sample of H II regions spans a range of galactocentric distance of nearly 10 kpc,  $3.4 < R < 13.7$  kpc. These distances depend upon the value of  $R_0$ , the galactocentric distance of the Sun. We assume  $R_0 = 8.5$  kpc for all our calculations. SMNDP found a nitrogen gradient of  $-0.09 \text{ dex kpc}^{-1}$ .

Extending the measurement of abundances to larger galactocentric distances is essential to our understanding of the abundance gradient and the chemical evolution of our Galaxy. In this paper we follow as closely as possible the method of SMNDP to measure the abundances in H II regions at galactocentric distances between 11.5 and 17.9 kpc. This expands the range over which the abundance gradient has been measured by almost 50%. This paper is only a preliminary report on this project, because of the limited data available on our two most

distant objects. Since SMNDP thoroughly discuss the issues involved in this kind of measurement, we limit our discussion to those particular areas where we differ from their analysis.

### II. OBSERVATIONS

Elemental abundances in some of the brighter H II regions in the Galaxy can easily be determined from optical spectroscopy alone. The derived abundances are sensitive to the values assumed for the electron temperature and density. The electron temperature is usually determined from the ratio of the line intensities of  $[\text{O III}] I(4363)/[I(4959) + I(5007)]$ , while the density is derived from the ratio of  $[\text{O II}] I(3727)/I(3729)$  or  $\text{S II } I(6717)/I(6730)$ . Since the 4363 Å line was generally not detected in the objects observed in this study, we attempted to measure the electron temperature via radio recombination line observations. We were unable to measure the ratio of the  $[\text{O II}]$  lines in any of our objects, and the  $[\text{S II}]$  line ratio proved to be very uncertain in most of the objects where we were able to measure it. Instead, radio continuum observations were used to estimate densities.

The objects and the positions at which they were observed are listed in Table 1. Also shown are their estimated galactocentric distances. These distances are all derived from the catalog of CO radial velocities by Blitz, Fich, and Stark (1982). This catalog tabulates the distances, where known, determined from optical spectrophotometric techniques. In Table 1, 11 of the objects (S212, S217, S219, S241, S271, S272, S283, S285, S298, S301, and BFS 54) have known optically determined distances, in all cases taken from the work of Moffat, Fitz-Gerald, and Jackson (1979).

The galactocentric distances of the remaining seven objects are kinematic distances calculated from CO radial velocities assuming a flat rotation curve at  $\Theta = 220 \text{ km s}^{-1}$ . Uncertainties in the kinematic distances are based upon the assumption that there is a  $7 \text{ km s}^{-1}$  uncertainty in the radial velocities. This corresponds to the observed size of the random motions of molecular clouds (Stark 1979). The uncertainty due to systematic effects, such as the use of an incorrect rotation curve and effects due to streaming motions, has not been included in the values shown in Table 1. These effects may provide up to

TABLE 1  
 OBJECT POSITIONS

OBJECT	POSITION (1950)		GALACTIC COORDINATES		$d$ (kpc)	$R$ (kpc)
	R.A.	Decl.	$l$	$b$		
S127	21 <sup>h</sup> 27 <sup>m</sup> 00 <sup>s</sup>	54°23'15"	96.27	2.60	11.5 ± 1.0	15.0 ± 0.9
S128	21 30 36	55 38 41	97.51	3.16	8.4 ± 0.8	12.7 ± 0.6
S209	4 07 18	51 02 00	151.60	-0.24	9.0 ± 2.4	17.0 ± 2.3
S211	4 32 57	50 46 40	154.64	2.44	6.0 ± 1.8	14.1 ± 1.8
S212	4 36 50	50 21 35	155.37	2.61	6.0 ± 0.6	14.2 ± 0.6
S217	4 54 46	47 53 50	159.15	3.26	5.2 ± 0.8	13.5 ± 0.6
S219	4 52 23	47 18 51	159.35	2.58	4.2 ± 0.6	12.5 ± 0.6
S241	6 00 43	30 22 45	180.76	4.16	4.7 ± 1.2	13.2 ± 1.2
S266	6 15 54	15 18 09	195.66	-0.10	9.6 ± 4.8	17.9 ± 4.7
S270	6 07 24	12 49 00	196.84	-3.11	5.9 ± 2.7	14.2 ± 2.7
S271	6 12 06	12 23 00	197.77	-2.31	4.8 ± 0.5	13.2 ± 0.5
S272	6 12 18	12 22 00	197.81	-2.28	4.8 ± 0.5	13.2 ± 0.5
S283	6 35 54	0 45 00	210.83	-2.56	9.1 ± 2.9	17.0 ± 2.8
S285	6 52 44	-0 27 15	213.83	0.62	6.9 ± 0.7	14.7 ± 0.7
S298	7 16 06	-13 08 00	227.75	-0.15	6.3 ± 2.5	13.6 ± 2.2
S301	7 07 41	-18 26 22	231.50	-4.41	5.8 ± 0.9	12.9 ± 0.8
BFS 54	6 44 18	1 22 00	211.25	-0.41	8.7 ± 2.8	16.3 ± 2.7
BFS 64	6 58 10	-8 47 00	221.85	-2.02	5.8 ± 0.9	11.7 ± 0.8

an additional 25% to the relative uncertainty in the distance to these seven objects, but this will add less than half of that to the uncertainty in galactocentric distance. The positions within the Galactic plane of all of the H II regions are shown in Figure 1.

#### a) Optical Spectroscopy

The optical spectroscopic data were obtained from 1985 December 6 to 10 with the Kitt Peak National Observatory<sup>1</sup> No. 2 36 inch (91 cm) telescope using the intensified Reticon scanner (IRS) and the white spectrograph. On the first four nights of the observations the largest area pair of apertures was

<sup>1</sup> The Kitt Peak National Observatory is part of the National Optical Astronomy Observatories, which is operated by the Association of Universities for Research in Astronomy, Inc., under contract with the National Science Foundation.

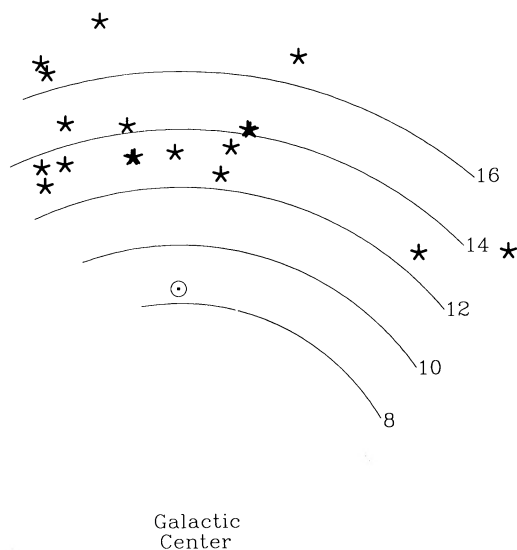


FIG. 1.—Positions of the H II regions observed (asterisks) and the Sun (Sun symbol) projected on the Galactic plane. Arcs showing the distance from the Galactic center are shown for 8, 10, 12, 14, and 16 kpc.

chosen (45" diameter, spaced 61"2 apart in the east-west direction). On the first three nights grating No. 26 was used at a tilt of 18°55' to obtain an effective resolution of 21 Å over wavelengths ranging from 4100 and 6800 Å. On the fourth night the same grating at a tilt of 17°37' provided the same resolution over the wavelength range 3300–6000 Å. On the fifth, and final, night grating 56 was used at a tilt of 30°53' to obtain an effective resolution of 5.6 Å over a wavelength range from 5800 to 7250 Å. A pair of rectangular apertures 35"6 by 14"2, again separated by 61"2, was used to obtain this improved spectral resolution.

Integration times were typically 600 s per individual spectrum. Virtually all of the observations were taken in "nebular mode," where it is assumed that the object is larger than the spacing between the two apertures and the telescope is moved to an "off" position after every observation on source. The "off" positions were typically 10' away and were chosen after examination of Palomar Sky Survey plates to locate areas of low emission. Short exposures of a comparison HeNeAr lamp (for wavelength calibration) and a quartz lamp (for flat-fielding) were taken at the beginning and end of each night's observations. Dark-current observations and observations of standard stars from the IRS Standard Star Manual (Barnes and Hayes 1984) were interspersed with the program observations.

Various instrumental and sky corrections were applied to the data using the IRAF package and the application program ONEDSPEC. After co-adding all of the spectra (between one and 10 spectra, typically four) obtained in a given instrument configuration for each object, the SPLIT routine was used to fit Gaussian line profiles to the spectra. The ratio of the intrinsic intensities of H $\alpha$  to H $\beta$  was assumed to be 2.859 throughout, and the extinction was calculated accordingly, using the standard extinction law of Seaton (1979). This value for the ratio of H $\alpha$  to H $\beta$  line intensities is a theoretical one for optically thin nebulae and varies by only a few percent over the entire likely range of density and temperature for our sample of H II regions. The extinction-corrected line intensities relative to H $\beta$  are shown in Table 2. The reddening correction at H $\beta$ ,

TABLE 2  
OPTICAL LINE INTENSITIES

LINE	OBJECT									
	S127	S128	S209	S221	S212	S217	S219	S241	S266	
[O II] $\lambda\lambda 3727, 3729$ .....	...	...	...	...	477.3	...	942.0	274.3	...	
He $\lambda 3970$ .....	...	...	...	...	13.0	...	21.3	...	...	
H $\delta$ $\lambda 4102$ .....	...	...	...	...	33.6	...	26.5	16.4	(12.9)	
H $\gamma$ $\lambda 4340$ .....	...	43.6	...	...	86.0	...	43.6	55.9	43.0	
He I $\lambda 4472$ .....	...	...	...	...	(5.1)	...	...	...	...	
H $\beta$ $\lambda 4861$ .....	100.0	100.0	...	100.0	100.0	100.0	100.0	100.0	100.0	
[O III] $\lambda 4959$ .....	...	87.5	...	...	23.8	...	...	...	...	
[O III] $\lambda 5007$ .....	...	264.1	...	...	79.0	...	...	...	(5.9)	
He I $\lambda 5876$ .....	...	13.2	...	...	12.2	...	...	...	4.1	
[O I] $\lambda 6300$ .....	...	3.1	...	17.6	5.6	17.4	...	...	...	
[N II] $\lambda 6548$ .....	20.4	17.2	...	33.9	25.1	30.3	...	35.8	...	
H $\alpha$ $\lambda 6563$ .....	285.9	285.9	285.9	285.9	285.9	285.9	285.9	285.9	285.9	
[N II] $\lambda 6584$ .....	89.8	44.1	43.5	102.7	66.8	83.0	94.2	85.8	18.1	
He I $\lambda 6678$ .....	...	10.2	...	...	9.2	...	...	...	...	
[S II] $\lambda 6717$ .....	30.0	10.1	...	21.5	21.7	52.5	67.1	...	49.2	2.9
[S II] $\lambda 6731$ .....	27.4	9.3	...	17.9	13.8				30.4	2.6
[Ar III] $\lambda 7136$ .....	...	10.2	(30.9)	...	10.9	32.5	...	...	...	
$C(H\beta)$ .....	1.51	2.63	...	2.93	1.81	1.50	1.30	1.27	2.50	
$\log F(H\beta)$ .....	-13.07	-12.37	...	-12.69	-12.37	-12.64	-12.47	-12.27	-11.60	

LINE	OBJECT									
	S270	S271	S272	S283	S285	S298	S301	BFS 54	BFS 64	
[O II] $\lambda\lambda 3727, 3729$ .....	...	...	...	...	...	...	...	...	...	
He $\lambda 3970$ .....	...	...	...	...	...	...	...	...	...	
H $\delta$ $\lambda 4102$ .....	...	...	...	...	...	29.5	...	...	...	
H $\gamma$ $\lambda 4341$ .....	...	...	...	...	...	50.2	55.7	39.1	...	
He I $\lambda 4472$ .....	...	...	...	...	...	...	...	...	...	
H $\beta$ $\lambda 4861$ .....	100.0	100.0	100.0	...	100.0	100.0	100.0	100.0	...	
[O III] $\lambda 4959$ .....	...	...	...	...	...	341.9	34.1	...	...	
[O III] $\lambda 5007$ .....	...	...	...	...	...	985.5	104.5	...	...	
He I $\lambda 5876$ .....	...	...	...	...	...	9.2	11.1	...	...	
[O I] $\lambda 6300$ .....	43.9	...	...	...	...	...	...	...	...	
[N II] $\lambda 6548$ .....	...	...	...	...	...	...	...	...	...	
H $\alpha$ $\lambda 6563$ .....	285.9	285.9	285.9	285.9	285.9	285.9	285.9	285.9	285.9	
[N II] $\lambda 6584$ .....	53.5	105.8	90.7	87.6	84.9	43.1	57.3	100.7	61.0	
He I $\lambda 6678$ .....	...	...	...	...	...	...	5.9	...	...	
[S II] $\lambda 6717$ .....	52.4	50.5	19.9	62.4	56.3	57.1	22.9	...	...	
[S II] $\lambda 6731$ .....		(8.0)	29.9						30.9	13.0
[Ar III] $\lambda 7136$ .....	...	...	...	...	...	...	...	...	17.9	
$C(H\beta)$ .....	2.68	1.95	2.69	...	1.53	1.46	1.11	0.85	...	
$\log F(H\beta)$ .....	-13.22	-12.78	-13.49	...	-12.75	-12.02	-11.76	-12.44	...	

$C(H\beta)$ , and the observed H $\beta$  flux,  $F(H\beta)$  (in ergs s<sup>-1</sup> cm<sup>-2</sup>), are also shown for each H II region.

#### b) Radio Observations

The electron temperature assuming LTE (denoted  $T_e^*$ ) can be estimated from the ratio of the integrated radio recombination line intensity to the continuum intensity at the same frequency. The true electron temperature ( $T_e$ ) deviates only slightly from this value. SMNDP showed that accounting for non-LTE effects required, on average, only a 3.6% correction for their data. Because of our choice of recombination line, we believe that our corrections will be even smaller. In view of the magnitude of the measurement uncertainty, we have ignored this correction, and accordingly we use  $T_e^*$  for  $T_e$  throughout our calculations.

The radio observations were made with the NRAO<sup>2</sup> Green Bank 140 foot (43 m) telescope between 1988 July 30 and August 8. We chose to observe H127 $\alpha$  at 3172.86 MHz and H159 $\beta$  at 3211.24 MHz. These particular lines minimize the expected non-LTE effects. At frequencies higher than that chosen, the emission is enhanced by stimulated emission. At frequencies lower than that chosen, pressure broadening decreases the measured emission. For the H II regions in our sample these competing effects balance at approximately 3 GHz. At these frequencies the beamwidth of the telescope is approximately 8'.

An S-band FET receiver with a system temperature of

<sup>2</sup> The National Radio Astronomy Observatory is operated by Associated Universities, Inc., under contract with the National Science Foundation.

TABLE 3  
RESULTS OF RADIO OBSERVATIONS

PROPERTY	OBJECT								
	S127	S209	S211	S212	S252	S284	S298	S301	S311
H127 $\alpha$									
$T_L$ (mK) .....	4 $\pm$ 2	68 $\pm$ 1	9 $\pm$ 2	12 $\pm$ 2	53 $\pm$ 3	13 $\pm$ 4	13 $\pm$ 2	28 $\pm$ 2	71 $\pm$ 2
$\Delta V$ (km s $^{-1}$ ) .....	(30)	28.4	32.2	33.8	23.4	21.5	33.6	23.7	22.9
$V$ (km s $^{-1}$ ) .....	(-76)	49.0	-31.0	-38.0	6.8	46.2	53.7	55.4	53.4
H159 $\beta$									
$T_L$ (mK) .....	...	15 $\pm$ 3	4 $\pm$ 2	...	16 $\pm$ 3	...	...	7 $\pm$ 2	20 $\pm$ 2
$\Delta V$ (km s $^{-1}$ ) .....	...	27.2	23.5	...	24.0	...	...	20.0	23.3
$V$ (km s $^{-1}$ ) .....	...	-48.6	-28.7	...	7.6	...	...	55.6	53.9
$T_c$ (K) .....	0.177	2.911	0.188	(0.43)	1.620	...	0.645	0.843	2.554

approximately 40 K was used with a 1024 channel digital correlator spectrometer. The correlator was split into four sections of 256 channels each, allowing two sections for the two polarizations centered at the H127 $\alpha$  line and two sections for the two polarizations at the H159 $\beta$  line. Each section of 256 channels was operated with a bandwidth of 10 MHz for a velocity resolution of 3.69 km s $^{-1}$ . The resulting spectra of the H II regions were fitted with Gaussian line profiles, and the results are shown in Table 3, where  $T_L$  and  $\Delta V$  are the best-fit peak line temperature and FWHM line width, respectively (values estimated or extremely uncertain are enclosed in brackets). Also listed are the continuum temperatures obtained at the same positions. These were obtained from the broad-band continuum measured at the 140 foot telescope while searching for the points of maximum continuum emission, where we also carried out the radio recombination line observations. A comparison of Table 1 and Table 3 shows that less than half our objects were detected in the H127 $\alpha$  recombination line. We have no optical spectra of two of the objects, S252 and S311 (W16). They were included in the radio observations only for comparison with SMNDP.

### III. ABUNDANCE ANALYSIS

#### a) Densities and Temperatures

The electron density ( $n_e$ ) for each object was estimated using radio continuum observations available in the literature, and the formula

$$n_e = 419 \left( \frac{S_\nu}{d\Theta^3} \right) \text{ cm}^{-3},$$

where  $S_\nu$  is the *total* (integrated over the entire object) radio continuum flux density at 3.17 GHz,  $d$  is the distance to the object in kiloparsecs, and  $\Theta$  is the angular diameter of the object in arcminutes. This formula is essentially that for the homogeneous sphere model of Mezger and Henderson (1967). The electron densities derived from this formula are the rms densities over the entire H II region and therefore are probably somewhat lower than the true densities of the emitting regions (perhaps by an order of magnitude), since the gas is not evenly distributed throughout the H II region. The higher density "clumps" contribute the greater part of the continuum emission. Although the densities are lower limits only, we show later that this should not be large enough to affect our results significantly. The excitation parameter ( $u$ ) of each of the H II

regions was estimated from

$$u = 15.1(S_\nu d^2)^{1/3} \text{ pc cm}^{-2},$$

which is derived using the same assumptions as above. The excitation parameter and electron density are shown in Table 4 (as well as the estimated total continuum flux density for each object).

The electron temperature ( $T_e^*$ ) was estimated by iteratively solving

$$\frac{\Delta V_L T_L}{T_c} = \frac{5.627 \times 10^4}{T_e^*(1.5 \ln T_e^* - 4.159)},$$

which is adapted from equation (1) of SMNDP. These results are also shown in Table 4. The three objects in common between this work and SMNDP (S252, S301, S311) have electron temperatures derived here that differ between the two studies by only 0.5  $\sigma$  on average. There are 12 H II regions for which no radio recombination line was detected, and thus no direct temperature determination was possible. Since the electron temperature of an H II region apparently varies with galactocentric distance—no doubt because of the abundance gradient in  $R$ —we have fitted the measured values against  $R$  as shown in Figure 2. We have included the data points from SMNDP (although we redetermined their values of  $R$ , since they assumed  $R_0 = 10$  kpc and we assume  $R_0 = 8.5$  kpc). Our best fit,

$$T_e^* = 3150 + 400R \text{ K},$$

is slightly less steep than the SMNDP fit. Although the data shows a very large scatter about this fitted line in the outer Galaxy, it should be noted that these data points also have very large uncertainties. Formally, the fit is actually quite good, but perhaps even more important, this is the only way we have of estimating temperatures in the H II regions where there are no direct measurements of temperatures. Accordingly we used this fit to estimate  $T_e^*$  for all the H II regions in our sample. This estimate appears as  $(T_e^*)_R$  in the last column of Table 4.

#### b) Abundance Calculations

Calculated ionic and atomic abundances are shown in Table 5. A five-level population model was used to estimate relative populations of the different energy levels in each ion. The atomic data for the model were taken from Baluja, Burke, and Kingston (1980), Berrington and Burke (1981), Krueger and

TABLE 4  
DERIVED DENSITY AND TEMPERATURE

Object	Diameter (arcmin)	$S_\nu$ (Jy)	Reference	$u$ (pc cm <sup>-2</sup> )	$n_e$ (cm <sup>-3</sup> )	$T_e^*$ (K)	$(T_e^*)_R$ (K)
S127	2	0.64	1	66.3	35.0	8800 <sup>+7500</sup> <sub>-2700</sub>	9900
S128	1.33	0.65	1	54.1	76.0	...	8900
S209	14	11.97	1	149.5	9.2	8800 <sup>+2200</sup> <sub>-1400</sub>	10800
S211	2	0.64	1	43.0	48.4	3800 <sup>+5200</sup> <sub>-1200</sub>	9500
S212	5	1.47	1	56.7	18.6	6700 <sup>+8100</sup> <sub>-2300</sub>	9500
S217	5.4	0.37	1	32.5	8.9	...	9200
S219	2.5	0.17	2	21.8	21.3	...	8800
S241	10	1.93	3	52.8	8.5	...	9100
S252	19	27.53	4	59.7	21.7	8100 <sup>+1000</sup> <sub>-1000</sub>	7700
S266	1.5	0.10	5	31.7	23.3	...	11100
S270	0.2	0.04	5	16.9	385.7	...	9500
S271	2	0.30	5	28.8	37.0	...	9100
S272	0.2	0.005	6	7.3	151.2	...	9100
S283	3	0.28	7	43.1	14.1	...	10800
S285	1.5	0.026	5	16.2	14.0	...	9700
S298	12	7.37	3	100.2	10.9	11900 <sup>+5200</sup> <sub>-2700</sub>	9300
S301	7	3.96	3	77.1	18.7	7700 <sup>+1400</sup> <sub>-1000</sub>	9000
S311	10	10.40	8	84.4	21.1	9200 <sup>+1400</sup> <sub>-1800</sub>	8100
BFS 54	3	0.12	5	31.5	9.5	...	10400
BFS 64	5	0.46	5	37.6	10.6	...	8400

REFERENCES.—(1) Kallas and Reich 1980; (2) Felli *et al.* 1978; (3) Felli and Churchwell 1972; (4) Day, Caswell, and Cooke 1972; (5) Fich, unpublished VLA observations; (6) Israel 1976; (7) Felli and Harten 1981; (8) Fich 1983.

Czyzak (1970), Mendoza (1983), Mendoza and Zeppen (1982), Nussbaumer and Rusca (1979), Nussbaumer and Storey (1981), Pradhan (1976), Pradhan (1978), Seaton (1975), and Zeppen (1982). The ionic abundances were calculated relative to hydrogen using a standard case B H $\beta$  line intensity for the densities and temperatures relevant to each object. Six of the H II regions that have optical data available also have values of  $T_e^*$  directly measured from the radio observations. Unfortunately, four of these objects (S127, S211, S212, and S298) have uncer-

tainties in  $T_e^*$  greater than 5000 K. Only two of these six objects (S209 and S301) have accurately measured  $T_e^*$ . For all the other objects in our sample we have used  $(T_e^*)_R$  in the abundance determination.

One does not, in general, have observations of all of the possible ionization stages for each atomic species. In order to convert these ionic abundances to atomic abundances, it was usually necessary to make some assumption about the appropriate ionization correction factor. SMNDP noted (with reference to the models of Stasinska 1980) that in high-excitation H II regions ( $u > 100$  pc cm<sup>-2</sup>) oxygen is primarily found as O<sup>++</sup> and the ratio O<sup>++</sup>/O<sup>+</sup> is approximately 4:1. In low-excitation H II regions ( $u < 50$  pc cm<sup>-2</sup>) the oxygen is primarily found as O<sup>+</sup>. The ionization correction scheme outlined by SMNDP relies on the ratio of O<sup>++</sup>/O<sup>+</sup>, and we accordingly use their scheme to produce the following rules to estimate oxygen and nitrogen abundances:

1. If  $u > 100$  pc cm<sup>-2</sup>, O<sup>+</sup> was not observed, and O<sup>++</sup> was detected, then the total oxygen abundance is estimated as 4/3 of the O<sup>++</sup> abundance.
2. If  $u > 100$  pc cm<sup>-2</sup> and either O<sup>+</sup> or O<sup>++</sup> was not detected, then the total nitrogen abundance is estimated to be 4 times the N<sup>+</sup> abundance (since the ionization correction factor is  $1 + \text{O}^{++}/\text{O}^+$ ).
3. If  $100 > u > 50$  pc cm<sup>-2</sup>, then the total nitrogen abundance is estimated to be twice the N<sup>+</sup> abundance.
4. If  $u < 50$  pc cm<sup>-2</sup>, then the total nitrogen abundance is taken to be the same as the N<sup>+</sup> abundance.

These corrections are only estimates and we have put an additional uncertainty factor into each of our derived quantities to account for this time (i.e., the lower uncertainty given for each abundance includes the result for the case when no ionization correction factor is applied). The uncertainties for

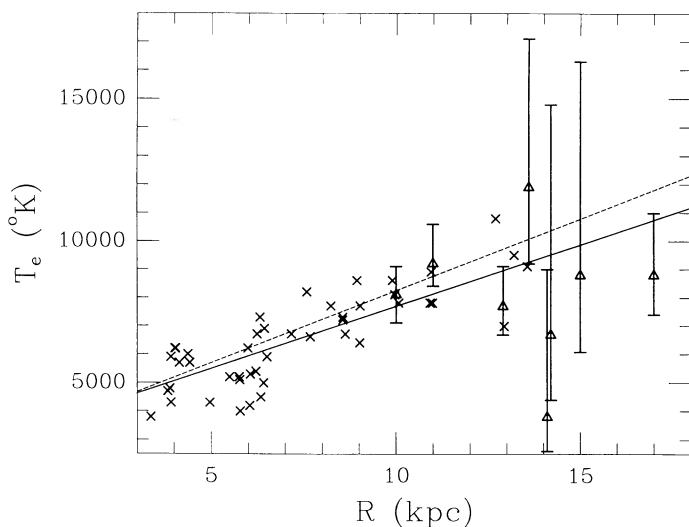


FIG. 2.—Electron temperatures ( $T_e$ ) of the SMNDP sample of H II regions shown as crosses, with galactocentric distances redetermined using  $R_0 = 8.5$  kpc. Newly measured  $T_e$  values are shown as open triangles with error bars. The dashed line is the SMNDP fit (rescaled in  $R$ ) to their data, and the solid line is our fit to all of the data.

TABLE 5  
RELATIVE ABUNDANCES<sup>a</sup>

SPECIES	OBJECT								
	S127	S128	S209	S211	S212	S217	S219	S241	S266
He II	...	0.095	...	...	0.089	...	...	...	0.031
O I	...	6.99 <sup>+0.27</sup> <sub>-0.30</sub>	...	7.64 <sup>+0.20</sup> <sub>-0.20</sub>	7.14 <sup>+0.22</sup> <sub>-0.22</sub>	7.69 <sup>+0.25</sup> <sub>-0.27</sub>	...	...	...
O II	...	...	...	...	8.35 <sup>+0.18</sup> <sub>-0.16</sub>	...	8.88 <sup>+0.23</sup> <sub>-0.21</sub>	8.20 <sup>+0.24</sup> <sub>-0.24</sub>	...
O III	...	8.17 <sup>+0.18</sup> <sub>-0.16</sub>	...	...	7.52 <sup>+0.20</sup> <sub>-0.20</sub>	...	<7.42 <sup>+0.21</sup> <sub>-0.21</sub>	<7.38 <sup>+0.22</sup> <sub>-0.22</sub>	6.20 <sup>+0.25</sup> <sub>-0.34</sub>
O	...	>8.03	...	...	8.43 <sup>+0.17</sup> <sub>-0.18</sub>	...	8.83 <sup>+0.23</sup> <sub>-0.21</sub>	8.20 <sup>+0.24</sup> <sub>-0.24</sub>	...
N II	7.18 <sup>+0.18</sup> <sub>-0.20</sub>	7.10 <sup>+0.14</sup> <sub>-0.13</sub>	7.08 <sup>+0.17</sup> <sub>-0.16</sub>	7.35 <sup>+0.12</sup> <sub>-0.11</sub>	7.20 <sup>+0.20</sup> <sub>-0.21</sub>	7.33 <sup>+0.19</sup> <sub>-0.20</sub>	7.42 <sup>+0.15</sup> <sub>-0.14</sub>	7.38 <sup>+0.16</sup> <sub>-0.15</sub>	6.43 <sup>+0.14</sup> <sub>-0.15</sub>
N	7.48 <sup>+0.18</sup> <sub>-0.52</sub>	7.40 <sup>+0.14</sup> <sub>-0.43</sub>	7.68 <sup>+0.14</sup> <sub>-0.76</sub>	7.35 <sup>+0.12</sup> <sub>-0.11</sub>	7.26 <sup>+0.19</sup> <sub>-0.22</sub>	7.33 <sup>+0.19</sup> <sub>-0.20</sub>	7.42 <sup>+0.15</sup> <sub>-0.14</sub>	7.45 <sup>+0.16</sup> <sub>-0.22</sub>	6.43 <sup>+0.14</sup> <sub>-0.15</sub>
S II	6.14 <sup>+0.19</sup> <sub>-0.21</sub>	5.80 <sup>+0.13</sup> <sub>-0.11</sub>	...	6.02 <sup>+0.16</sup> <sub>-0.15</sub>	5.97 <sup>+0.29</sup> <sub>-0.46</sub>	6.17 <sup>+0.12</sup> <sub>-0.11</sub>	6.34 <sup>+0.17</sup> <sub>-0.16</sub>	6.36 <sup>+0.13</sup> <sub>-0.12</sub>	5.00 <sup>+0.12</sup> <sub>-0.12</sub>
Ar III	...	6.11 <sup>+0.14</sup> <sub>-0.13</sub>	...	...	6.07 <sup>+0.22</sup> <sub>-0.27</sub>	6.58 <sup>+0.14</sup> <sub>-0.14</sub>	...	...	...
Ar	...	6.29 <sup>+0.14</sup> <sub>-0.31</sub>	...	...	6.24 <sup>+0.22</sup> <sub>-0.44</sub>	6.76 <sup>+0.15</sup> <sub>-0.32</sub>	...	...	...

<sup>a</sup> Except He II, expressed as  $(12 + \log X/H)$ .

SPECIES	OBJECT								
	S270	S271	S272	S283	S285	S298	S301	BFS 54	BFS 64
He II	...	...	...	...	...	0.068	0.777	...	...
O I	8.03 <sup>+0.22</sup> <sub>-0.23</sub>	...	...	...	...	...	...	...	...
O II	...	...	...	...	...	...	...	...	...
O III	...	...	...	...	...	8.68 <sup>+0.13</sup> <sub>-0.12</sub>	8.02 <sup>+0.21</sup> <sub>-0.18</sub>	...	...
O	...	...	...	...	...	8.80 <sup>+0.12</sup> <sub>-0.24</sub>	>7.84	...	...
N II	7.08 <sup>+0.14</sup> <sub>-0.14</sub>	7.43 <sup>+0.14</sup> <sub>-0.12</sub>	7.36 <sup>+0.13</sup> <sub>-0.11</sub>	7.15 <sup>+0.09</sup> <sub>-0.08</sub>	7.26 <sup>+0.11</sup> <sub>-0.10</sub>	7.01 <sup>+0.16</sup> <sub>-0.15</sub>	7.38 <sup>+0.16</sup> <sub>-0.14</sub>	7.25 <sup>+0.09</sup> <sub>-0.08</sub>	7.29 <sup>+0.13</sup> <sub>-0.12</sub>
N	7.08 <sup>+0.14</sup> <sub>-0.14</sub>	7.43 <sup>+0.14</sup> <sub>-0.12</sub>	7.36 <sup>+0.13</sup> <sub>-0.11</sub>	7.15 <sup>+0.09</sup> <sub>-0.08</sub>	7.26 <sup>+0.11</sup> <sub>-0.10</sub>	7.61 <sup>+0.16</sup> <sub>-0.75</sub>	7.38 <sup>+0.16</sup> <sub>-0.44</sub>	7.25 <sup>+0.09</sup> <sub>-0.08</sub>	7.29 <sup>+0.13</sup> <sub>-0.12</sub>
S II	6.17 <sup>+0.15</sup> <sub>-0.15</sub>	6.14 <sup>+0.18</sup> <sub>-0.18</sub>	6.20 <sup>+0.20</sup> <sub>-0.21</sub>	6.07 <sup>+0.19</sup> <sub>-0.23</sub>	6.33 <sup>+0.14</sup> <sub>-0.13</sub>	6.20 <sup>+0.13</sup> <sub>-0.12</sub>	6.23 <sup>+0.19</sup> <sub>-0.17</sub>	...	6.48 <sup>+0.14</sup> <sub>-0.12</sub>
Ar III	...	...	...	...	...	...	...	...	...
Ar	...	...	...	...	...	...	...	...	...

all abundances shown in Table 5 also include a contribution for a 1000 K uncertainty [derived from the uncertainty in the fitted  $(T_e^*)_R$  relation] in the value of  $(T_e^*)_R$  used plus an additional factor due to the uncertainty in the derived electron density. None of these results in a symmetric uncertainty, as is probably most evident in the object S209. The nitrogen abundance of that object is given as  $7.71^{+0.14}_{-0.76}$  where the large negative uncertainty reflects primarily the  $N$  abundance if no ionization correction factor is applied to the  $N^+$  abundance.

The sulfur abundances cannot be accurately predicted from our data, since we did not detect the  $S^{++}$  line at 6312 Å. SMNDP found that  $S^{++}$  was usually the dominant form of sulfur and there is no straightforward way to estimate total sulfur abundance with the information available to us. For argon we have used the same correction factor as SMNDP, namely, that the argon abundance is 1.5 times the  $Ar^{++}$  abundance, although this is not a very reliable estimate. The helium abundance has been estimated using the He I 5876 Å line,  $T_e^*$ , and the formula from Barker (1978):

$$y = (0.493 + 0.305t - 0.059t^2) \frac{I(5786)}{I(H\beta)},$$

where  $y$  is the  $He^+$  abundance and  $t$  is the temperature in  $10^4$  K. Since this recombination line ratio measures the amount of  $He^+$ , it only provides a lower limit to the total helium abun-

dance. We have no data with which to estimate the amount of neutral helium.

The results of these calculations are fairly consistent, with one major exception. The object S266 is listed with extremely low abundances in all of the elements. We are certain that this is due to a substantial underestimate of the electron density. From VLA observations Fich (1987) identified this object as a shell source probably driven by a strong stellar wind. The electron density is estimated to be in excess of  $10^6 \text{ cm}^{-3}$ , not  $23.3 \text{ cm}^{-3}$  as we have used, and thus the abundances listed here for that object are not to be trusted.

### c) Temperature and Density versus Abundance

The abundance determined from forbidden-line emission is strongly dependent on the temperature assumed for the nebula. We have used a directly measured temperature for only two of our objects. In all of the other objects we have relied upon a temperature interpolated from a linear fit of temperature versus galactocentric distance. The gradient of this temperature relation therefore plays a central role in setting the abundance gradient measured.

The major result of this paper (see below) is that the nitrogen abundance is unexpectedly high in the outer Galaxy. If this is mistaken, it would most likely be due to an underestimate of the temperatures. Higher temperatures would imply lower

abundances. However, we believe that it is more likely that we have erred in the opposite direction. Our fitted temperature relation (shown in Fig. 2) is above the measured values for most of the objects at large galactocentric distances.

Moreover, the abundance depends on temperature in a non-linear fashion. To reduce the nitrogen abundances by a factor of 2 (as would be the minimum required) would require that the temperature be nearly 4000 K higher in the majority of the objects. This does not seem likely.

Some analyses of H II region abundances use the temperature models as in the method developed by Peimbert (1967) that provides for temperature fluctuations. The use of this method would produce higher abundances than those we have determined.

The other parameter used in deriving the abundances from the observed intensities is the electron densities. As mentioned earlier, we expect that our density estimates (which assume a homogeneous nebula) are low by up to a factor of 10 as a result of clumpiness in the H II regions. We tried the experiment of using densities 100 times greater than our measured values. The largest effect was seen in the  $O^+$  abundances, which increased by only 15%. A slightly smaller effect was seen in the  $S^+$  abundances, and there was no significant effect on the other abundances.

#### IV. DISCUSSION

The principal results of this work are shown in Figures 3, 4, and 5, where the abundances of  $S^+$ , O, and N, respectively, are plotted against galactocentric distance. In these figures our results are plotted in heavy lines, while the SMNDP results are plotted with lighter lines. The  $S^+$  abundances do not show any trend with galactocentric distance, consistent with the results of SMNDP. Our O abundances also do not add anything new, primarily because we have no detections or good abundance limits for the most distant of our objects. However, the nitrogen abundances (Fig. 5) are substantially different from what we expected.

Virtually all of the newly measured nitrogen abundances are greater than that expected from an extrapolation of the

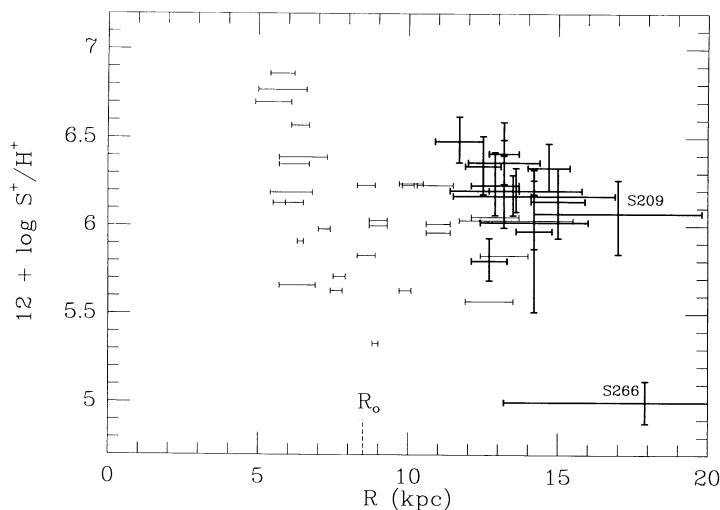


FIG. 3.—Abundances of  $S^+$  relative to hydrogen plotted against the galactocentric distance. Data from SMNDP are plotted with light lines, while our data are shown with heavier lines. Two of the more distant objects (S209 and S266) are labeled and discussed in the text.

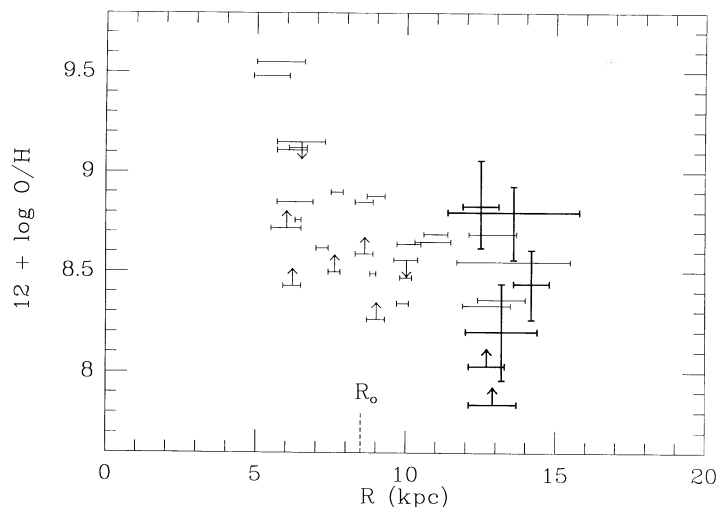


FIG. 4.—Abundances of O relative to hydrogen plotted against the galactocentric distance. Data from SMNDP are plotted with light lines, while our data are shown with heavier lines.

SMNDP nitrogen gradient fit, which itself has a shallower slope than many others in the literature. A  $\chi^2$  analysis (slightly complicated by the fact that there are measurement uncertainties in both variables; see discussion in the Appendix of Fich, Blitz, and Stark 1989 and extensive references to the necessary techniques in Kalantar 1989) rules out the SMNDP line at the  $5.0 \sigma$  level with all of the data or at the  $6.9 \sigma$  level when the object S266 is removed. Our results are consistent with a flat gradient in the nitrogen abundance outside of  $R_0$ . In fact, it would be easy to argue for a step-function nitrogen gradient. Within the Solar Circle the abundance is greater than 8.0 dex ( $12 + \log X/H$ , where  $X/H$  is the abundance relative to hydrogen), while it is approximately 7.3 dex farther out. A similar result has been pointed out by Lester *et al.* (1987), who obtained the ratio  $N^{++}/O^{++}$  in H II regions from infrared observations. They noted that this ratio is very large, but vari-

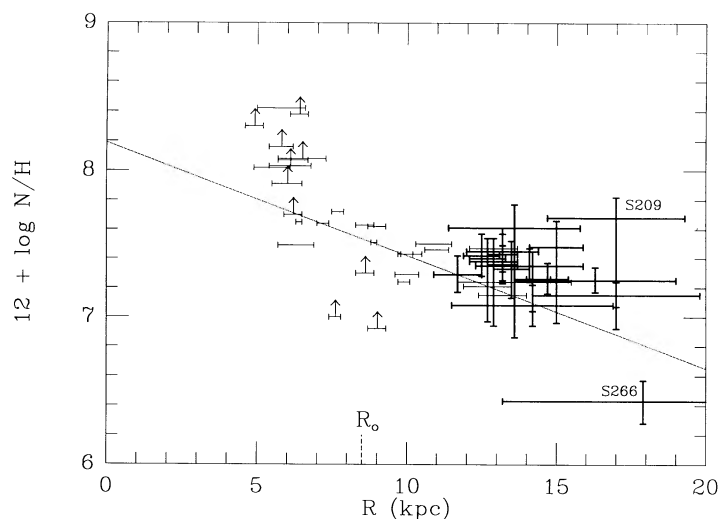


FIG. 5.—Abundances of N relative to hydrogen plotted against the galactocentric distance. Data from SMNDP are plotted with light lines, while our data are shown with heavier lines. Two of the more distant objects (S209 and S266) are labeled and discussed in the text. The best fit from SMNDP is shown (rescaled from their  $R_0 = 10$  kpc to our  $R_0 = 8.5$  kpc) by the line across the plot.

able between objects, inside 7 kpc and small for all objects outside this distance.

The two highest nitrogen abundance objects (S209 and S298) may not be good representative objects. The first, S209, has an extremely uncertain abundance, as mentioned in § IIIb, and the second, S298, has been identified as containing a nitrogen-rich Wolf-Rayet star (Smith 1968).

There has been much discussion in the literature as to the origin of nitrogen in the interstellar medium. Originally it was thought to be of secondary origin; that is, the nitrogen is formed by the processing of a primary element (such as carbon or oxygen) that is formed directly from hydrogen and helium). Not only are there doubts about this proposition, but other complicating factors have been suggested. The relative amounts of oxygen and nitrogen probably depend on the slope of the initial mass function (IMF), since oxygen is mostly produced in massive stars, while nitrogen is mostly produced in intermediate-mass stars. It has been suggested that the IMF may vary with galactocentric distance (Garmany, Conti, and Chiosi 1982). It has also been suggested that the IMF is bimodal, with one IMF for massive stars and another for lower mass stars (see a recent review by Silk 1988). If this is true, each mode of the IMF could certainly have an independent variation with galactocentric distance. Further discussions of the

theoretical and observational problem of the origin of nitrogen are given by Matteucci (1986) and Pagel (1987).

Comparing our results with the nitrogen abundance seen in other galaxies requires extra care because of a number of selection effects. One particularly insidious problem is that most of the H II regions in our sample are quite small, low-excitation H II regions that might not even be detected in another galaxy. It is possible that much of the work done on external galaxies can only be compared with the abundance gradient in what we refer to as the "inner Galaxy."

There is much room for continued work in this area, especially in determining the oxygen abundances in the most distant H II regions. Of high priority would be further  $T_e$  measurements from radio recombination lines. It will be interesting to see whether the oxygen abundances follow as unexpected a trend as those of nitrogen.

Much of this work was carried out while M. F. was a visitor at the Canadian Institute for Theoretical Astrophysics. M. S. appreciates time off from her regular work to follow more esoteric pursuits. We thank Marshall McCall for a careful reading of an early draft of this paper and the contribution of several very useful suggestions.

#### REFERENCES

- Baluja, K. L., Burke, P. G., and Kingston, A. E. 1980, *J. Phys. B*, **13**, L543.  
 Barker, T. 1978, *Ap. J.*, **220**, 193.  
 Barnes, J. V., and Hayes, D. S. 1984, *IRS Standard Star Manual* (Tucson: KPNO).  
 Berrington, K. A., and Burke, P. G. 1981, *Planet. Space Sci.*, **29**, 377.  
 Blitz, L., Fich, M., and Stark, A. A. 1982, *Ap. J. Suppl.*, **49**, 183.  
 Day, G. A., Caswell, J. L., and Cooke, D. J. 1972, *Australian J. Phys. Ap. Suppl.*, **25**, 1.  
 Felli, E., and Churchwell, E. 1972, *Astr. Ap. Suppl.*, **5**, 369.  
 Felli, E., and Harten, R. 1981, *Astr. Ap.*, **160**, 28.  
 Felli, E., Harten, R., Habing, H., and Israel, F. P. 1978, *Astr. Ap. Suppl.*, **32**, 423.  
 Fich, M. 1983, Ph.D. thesis, University of California, Berkeley.  
 ———. 1987, *Bull. AAS*, **19**, 717.  
 Fich, M., Blitz, L., and Stark, A. A. 1989, *Ap. J.*, **342**, 272.  
 Garmany, C. D., Conti, P. S., and Chiosi, C. 1982, *Ap. J.*, **263**, 777.  
 Hawley, S. A. 1978, *Ap. J.*, **224**, 417.  
 Israel, F. P. 1976, *Astr. Ap.*, **52**, 175.  
 Kalantar, A. H. 1989, *Comput. Phys.*, **3** (No. 9), 10.  
 Kallas, E., and Reich, W. 1980, *Astr. Ap. Suppl.*, **42**, 227.  
 Krueger, Y. K., and Czyzak, S. J. 1970, *Proc. Roy. Soc. London, A*, **318**, 531.  
 Lester, D. F., Dinerstein, H. L., Werner, M. W., Watson, D. M., Genzel, R., and Storey, J. W. V. 1987, *Ap. J.*, **320**, 573.  
 Matteucci, F. 1986, *Pub. A.S.P.*, **98**, 973.  
 Mendoza, C. 1983, in *IAU Symposium 103, Planetary Nebulae*, ed. D. R. Flower (Dordrecht: Reidel), p. 143.  
 Mendoza, C., and Zeppen, C. J. 1982, *M.N.R.A.S.*, **198**, 127.  
 Mezger, P. G., and Henderson, A. P. 1967, *Ap. J.*, **147**, 471.  
 Moffat, A. F. J., FitzGerald, M. P., and Jackson, P. D. 1979, *Astr. Ap. Suppl.*, **38**, 197.  
 Nussbaumer, H., and Rusca, C. 1979, *Astr. Ap.*, **72**, 129.  
 Nussbaumer, H., and Storey, P. J. 1981, *Astr. Ap.*, **99**, 177.  
 Pagel, B. E. J. 1987, in *The Galaxy*, ed. G. Gilmore and B. Carswell (Dordrecht: Reidel), p. 341.  
 Peimbert, M. 1967, *Ap. J.*, **150**, 825.  
 Peimbert, M., Torres-Peimbert, S., and Rayo, J. F. 1978, *Ap. J.*, **220**, 516.  
 Pradhan, A. K. 1976, *M.N.R.A.S.*, **177**, 31.  
 ———. 1978, *M.N.R.A.S.*, **183**, 89P.  
 Searle, C. L. 1971, *Ap. J.*, **168**, 327.  
 Seaton, M. J. 1975, *M.N.R.A.S.*, **170**, 475.  
 ———. 1979, *M.N.R.A.S.*, **187**, 73P.  
 Shaver, P. A., McGee, R. X., Newton, L. M., Danks, A. C., and Pottasch, S. R. 1983, *M.N.R.A.S.*, **204**, 53 (SMNDP).  
 Silk, J. 1988, in *Galactic and Extragalactic Star Formation*, ed. R. E. Pudritz and M. Fich (Dordrecht: Kluwer), p. 503.  
 Smith, L. F. 1968, *M.N.R.A.S.*, **138**, 109.  
 Stark, A. A. 1979, Ph.D. thesis, Princeton University.  
 Stasinska, G. 1980, *Astr. Ap.*, **84**, 320.  
 Zeppen, C. J. 1982, *M.N.R.A.S.*, **198**, 111.

MICHEL FICH: Physics Department, University of Waterloo, Waterloo, Ontario, Canada N2G 3L1

MARIABETH SILKEY: Hatfield and Dawson Consulting Electrical Engineers, 4226 Sixth Avenue, N.W., Seattle, WA 98107